Photoresponsive nanoscale columnar transistors

Xuefeng Guo[a,1], Shengxiong Xiao[b], Matthew Myers[b], Qian Miao[c], Michael L. Steigerwald[b], and Colin Nuckolls[b,1]

[a]Center for Nanochemistry, Beijing National Laboratory for Molecular Sciences, State Key Laboratory for Structural Chemistry of Unstable and Stable Species, College of Chemistry and Molecular Engineering, Peking University, Beijing 100871, People's Republic of China; [b]Department of Chemistry and the Columbia University Center for Electronics of Molecular Nanostructures, Columbia University, New York, NY 10027; and [c]Department of Chemistry, The Chinese University of Hong Kong, Shatin, New Territories, Hong Kong, China

Edited by Harry B. Gray, California Institute of Technology, Pasadena, CA, and approved December 4, 2008 (received for review August 2, 2008)

This study reports a general methodology for making stable high-performance photosensitive field effect transistors (FET) from self-assembled columns of polycyclic aromatic hydrocarbons by using single-walled carbon nanotubes (SWNTs) as point contacts. In particular, the molecules used in this work are liquid crystalline materials of tetra(dodecyloxy)hexabenzocoronenes (HBCs) that are able to self-organize into columnar nanostructures with a diameter similar to that of SWNTs and then form nanoscale columnar transistors. To rule out potential artifacts, 2 different structural approaches were used to construct devices. One approach is to coat thin films of HBCs onto the devices with the SWNT–metal junctions protected by hydrogensilsesquioxane resin (HSQ), and the other is to place a droplet of HBC exactly on the nanogaps of SWNT electrodes. Both types of devices showed typical FET behaviors, indicating that SWNT–molecule–SWNT nanojunctions are responsible for the electrical characteristics of the devices. After thermally annealing the devices, HBC molecules assembled into columnar structures and formed more efficacious transistors with increased current modulation and higher gate efficiency. More interestingly, when the devices were exposed to visible light, photocurrents with an on/off ratio of >3 orders of magnitude were observed. This study demonstrates that stimuli-responsive nanoscale transistors have the potential applications in ultrasensitive devices for environmental sensing and solar energy harvesting.

chemistry | field effect transistor | nanofabrication | nanoscience | self-assembly

Fabrication of molecule-scaled transport junctions that enable the measurement of the electrical characteristics of a small numbers of molecules could be of substantial importance to the improvement of molecular electronics. Recent years have witnessed the significant progress in molecular electronics, exemplified by a comprehensive set of proof-of-concept experiments (1–6). In this area, the big challenge is still the construction, measurement, and understanding of the current–voltage responses of the electronic circuits in which molecular systems play an important role as conducting elements. Because single-walled carbon nanotubes are quasi-1D ballistic conductors that have the molecule-scale width and length suitable for nanofabrication and the wealth of optoelectronic properties (7–17) they have demonstrated potential applications as fundamental building blocks in nanoelectronic and nanophotonic devices and offer substantial promise for integrated nanosystems. In particular, they could be, in principle, the ideal electrodes having significant advantages over metal electrodes for testing molecular conductance.

Recently we and others (9, 16, 18–22) have developed different methods for forming the nanogaps for electrical attachment of single molecules onto the ends of carbon nanotubes, thus permitting single-walled carbon nanotubes (SWNTs) as electrodes to enrich the measurements of single molecules. In our system, carboxylic acid-functionalized nanogaps are formed from SWNTs by ultrafine electron beam lithography and precise oxygen plasma etching. This allows molecules to be wired into the SWNT circuits through robust amide linkages, avoiding the inherent problems related to thiol molecules inserted between gold electrodes. The amide linkages are so robust that the devices can endure external stimuli and chemical treatments. Using this method, we have tested a number of different types of molecular wires. We have made different types of molecular electronic devices that are able to switch the conductance as a function of pH (18), detect the binding between protein and substrate (19), photoswitch the conductance between conjugated and nonconjugated states (20), measure the conductance differences between complementary and mismatched DNA strands (21), and sense the existence of electron-deficient molecules (22).

In our lab, another major interest is to develop a class of polycyclic aromatic hydrocarbons that are readily self-assembled or self-healed to form self-complementary columnar liquid crystalline phases. Recently, we reported the synthesis of contorted tetra(dodecyloxy)hexabenzocoronene (HBC) **1** (Fig. 1*A*) (23). The molecular substructure of **1** represents the intersection and fusion of 3 pentacene subunits. Relatively high carrier mobilities and current modulation (u = 0.02 cm^2/V·s; on–off current ratio of 10^6:1) were observed in field effect transistors made with liquid crystalline films (23), self-assembled monolayers (22), and nanostructured cables (24). Because of the coexistence of the inner π-system as a conductive core and the outer π-system as an insulating sheath (Fig. 1*A*), the path of charge transport is dominated by intracolumnar transport through the 1D radialence core (25).

In this work, we detailed a method to incorporate the self-assembly properties of HBC with SWNT electrodes to make efficacious field-effect nanotransistors that are sensitive to their external stimuli. The molecules used in this work are liquid crystalline materials of HBCs that are able to self-organize into columnar nanostructures with a diameter similar to that of SWNTs. As a result, nanoscale columnar transistors are formed when ultrasmall point contacts separated by molecular-length scales are used as the source and drain electrodes and bridged by individual columnar structures. To rule out the artifacts, 2 device architectures were developed. One is to form thin films of HBCs on the devices with SWNT–metal junctions covered by HSQ (Fig. 1*B*) and the other is to place a very small droplet of HBCs onto only the nanogaps of SWNT electrodes without contact with the metal pads (Fig. 1*C*). Devices made by using either method show typical field effect transistor (FE) properties, suggesting that SWNT–molecule–SWNT nanojunctions are responsible for the electronic characteristics. For all working devices, after thermal annealing or exposure to visible light, significant increases in channel conductivity were observed. This

Author contributions: X.G. and C.N. designed research; X.G., S.X., M.M., and Q.M. performed research; X.G. contributed new reagents/analytic tools; X.G., M.L.S., and C.N. analyzed data; and X.G., S.X., M.M., Q.M., M.L.S., and C.N. wrote the paper.

The authors declare no conflict of interest.

This article is a PNAS Direct Submission.

[1]To whom correspondence may be addressed. E-mail: guoxf@pku.edu.cn or cn37@columbia.edu.

This article contains supporting information online at www.pnas.org/cgi/content/full/0807596106/DCSupplemental.

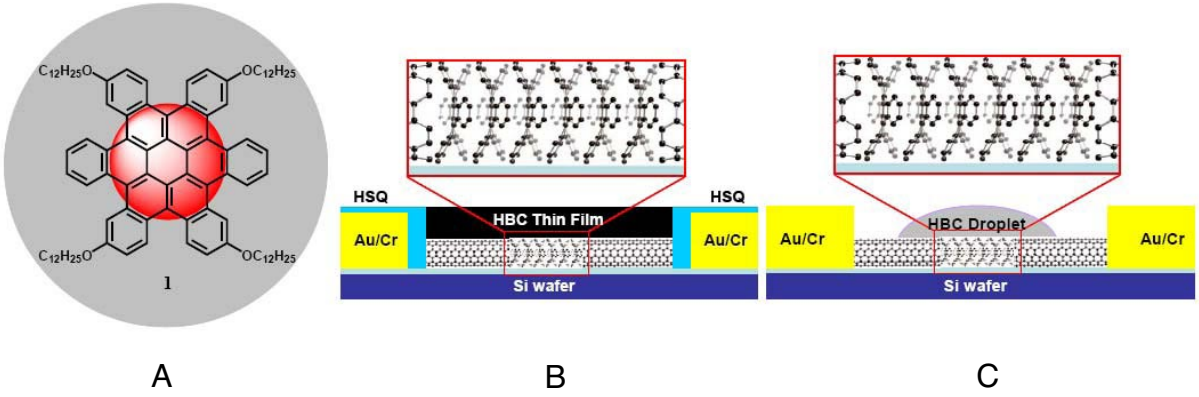

Fig. 1. A schematic of how HBCs can be assembled to form nanoscale columnar transistors and measured by SWNT point contacts. (*A*) The structure of contorted liquid crystalline tetra(dodecyloxy)hexabenzocoronene (HBC) 1. (*B*) Device structure of single-column transistors with SWNT–metal junctions protected by HSQ. (*C*) Device structure of single-column transistors made by drop casting. Only the nanogaps between SWNT electrodes are covered by HBCs.

study forms the basis for new types of ultrasensitive stimuli-responsive molecular devices.

Results and Discussion

Device Fabrication. SWNT transistors are made through the procedure described before (18–22). Fig. 2 shows a schematic and micrograph of the devices used. Briefly Au (50 nm) on Cr (5 nm) leads, which are separated by 20 μm, form the source and drain contacts to an individual single-walled carbon nanotube. Then the tubes are oxidatively cut by using ultrafine e-beam lithography and precise oxygen plasma that produces the nanogaps of 1–10 nm on the nanotube ends. In our previous studies, we have made a number of different molecular electronic devices (17–22). It is in this gap that we also self-assembled monolayers of HBCs to form monolayer transistors that can sense the existence of electron-deficient molecules. In this study, we intend to insert columnar structures of HBCs into the nanogaps to form nannoscale columnar transistors. By applying the S/D bias voltage to metal contacts attached to the nanotubes and the gate bias voltage to the doped silicon as global back-gate electrode, we can tune the carrier density in the devices by irradiation with visible light.

Previous studies have showed that HBC derivatives exhibit high carrier mobility and large current modulation in FETs formed from liquid crystalline thin films (23), self-assembled monolayers (22), and nanostructured cables (24). In this study, there are 2 possible pathways for charge transport. The first is the traditional way through the junctions between Au electrodes and

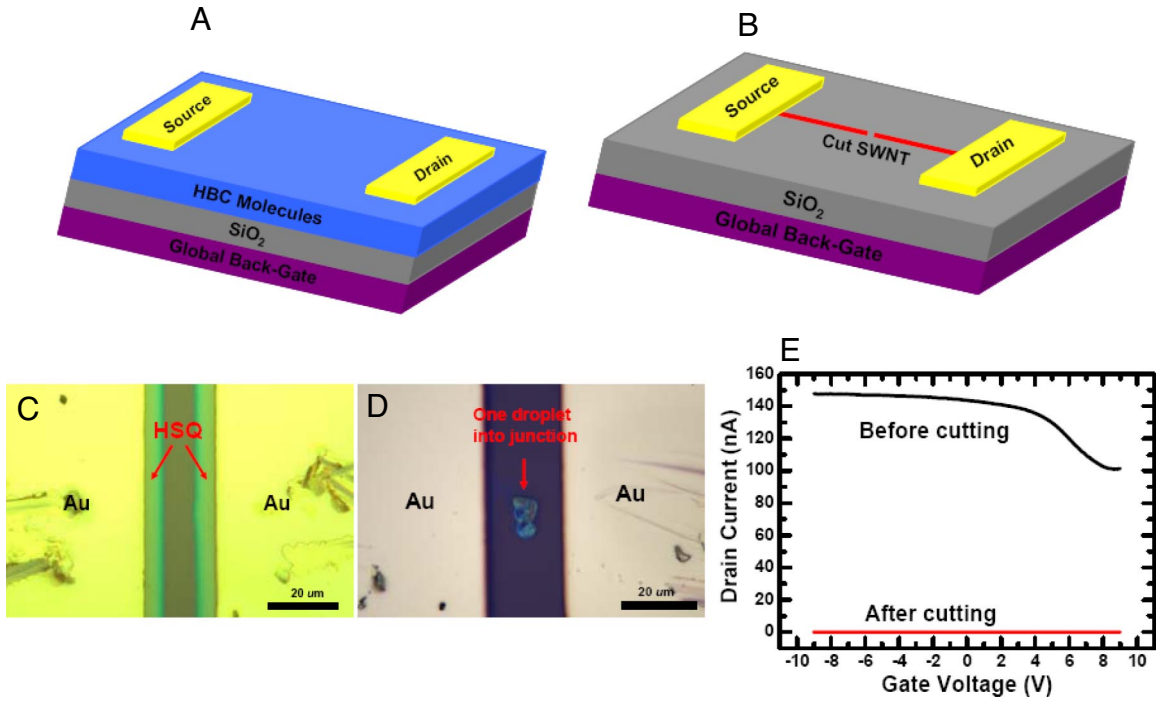

Fig. 2. Device structure formed by cutting an individual metallic SWNT. (*A*) A general field effect transistor with HBC thin films as the active semiconducting layers. (*B*) A cut SWNT transistor connected by large metal leads as the S/D electrodes and the silicon wafer as the global back-gate. (*C*) An optical micrograph of a device whose SWNT–metal junctions have been protected by HSQ. (*D*) An optical micrograph of a device made by drop-casting HBCs exactly on the nanogaps. (*E*) Electrical characteristics of a metallic tube (I_D vs. V_G at V_D = 50 mV) used for testing before (black curve) and after (red curve) oxidative cutting.

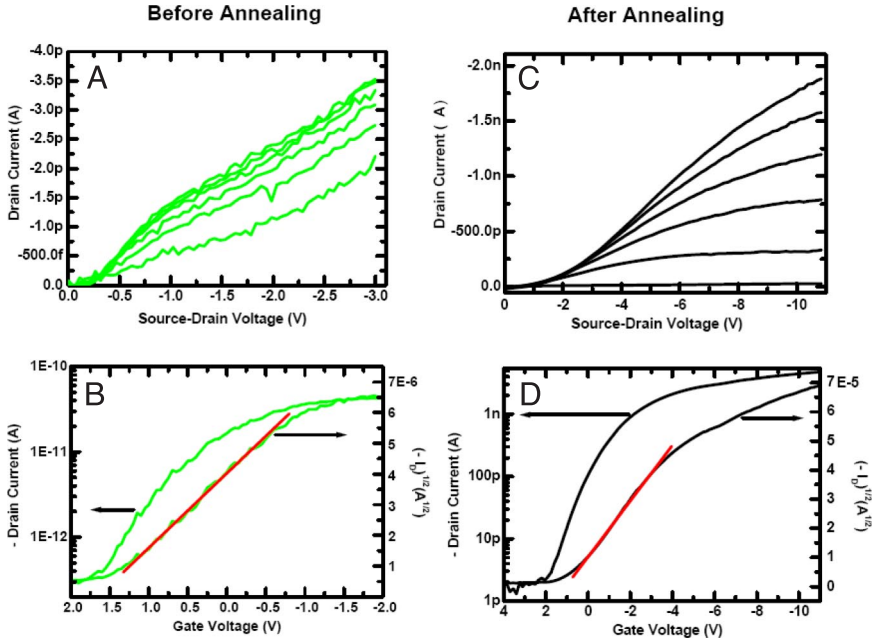

Fig. 3. Device characteristics of the same device measured in Fig. 2*E* before and after annealing. (*A*) Transistor output, $V_G = 0$ to -3 V in 0.6-V steps. (*B*) Transfer characteristics for the device, $V_D = -3$ V. (*C*) Transistor output, $V_G = 0$ to -11 V in 2.2-V steps for the same device after the treatment of heat. (*D*) Transfer characteristics for the device, $V_D = -11$ V.

HBC thin films in a device as shown in Fig. 2*A* and the other is through the junctions between cut SWNTs and HBC molecules (Fig. 2*B*). To exclude the first possibility, 2 different approaches were implemented (Fig. 1 *B* and *C*). In the case of Fig. 1*B*, cut SWNT transistors are formed by our previous procedure (18–22), followed by using e-beam lithography again to protect the metal–SWNT junctions with HSQ resin. Fig. 2*C* shows an optical micrograph of the devices used. Thin film transistors are made by spin-casting HBC thin films (Fig. 1*B*). In the other case of Fig. 1*C*, after the nanotubes are fully cut, a tiny drop (≈10 μm in size) of a 1,2-dichloroethane solution of HBCs is introduced into the nanogaps by using a picospritzer. Fig. 2*D* shows an optical micrograph of the typical device structure used. It is very clear from this image that the tiny drop of organic semiconducting materials is not connected to any Au electrode. In both of the cases, charge transport passes exclusively through SWNT–molecule–SWNT junctions.

Depending on the different diameter and chirality of the tubes, SWNTs can be either metallic or semiconducting. Before cutting, we scan the current–voltage characteristics of SWNT transistors and then categorize them as metallic or semiconducting. To aid in the subsequent analysis of the devices, we always choose those that are made form metallic SWNTs (lack of gate dependence). Fig. 2*E* shows the comparison of the electrical properties of a metallic tube device before and after cutting. Before cutting, the electrical resistance of this device is ≈0.34 MΩ, and after cutting the device is open with the current down to the noise limit of the equipment (<2 pA).

Thermal Optimization. We measured the electrical properties of the as-formed devices by either spin-coating or drop-casting techniques as shown in Fig. 1 *B* and *C*. All of the working devices behaved as *p*-type semiconductors. Fig. 3 shows the transistor characteristics for the same device characterized in Fig. 2*E* made by spin-coating in Fig. 1*B*. Similar data are available for a device made by drop-casting in Fig. 1*C* [see supporting information (SI) *Text*]. These experimental results thoroughly identify that the current path of the devices is through SWNT electrodes connected by HBCs. These devices are stable, and their properties do not degrade after many measurement cycles.

Fig. 3 also shows the comparison of the electrical characteristics of the same device before and after annealing. Before annealing, we found that the number of devices exhibiting FET behaviors was low (≈10%, ≈120 devices used), and the maximum current within the measured scale is relatively small as shown in Fig. 3 *A* and *B*. However, after a single heating/cooling cycle, the yield of the working devices increased significantly to ≈60%. Another significant difference is the maximum current after annealing, which increased by a factor of >2 orders at $V_D = -3$ V. These imply that with the aid of heat, liquid crystalline HBC **1** (23) can be transformed to their intermediate states, which are supposed to self-organize into ordered columnar liquid crystalline phases composed of molecular stacks that orient themselves parallel to the nanogaps between carbon nanotubes, thus enhancing the yield of the working devices and favoring the charge transport through SWNT point contacts. Once nanoscale columns are formed to bridge the cut carbon nanotube electrodes and then nanoscale columnar transistors are formed, it is reasonable that these columnar bridges could dominate the carrier transport characteristics of the devices. Because the diameter of these self-assembled columns (≈2.8 nm for **1** with its side chains fully extended) is larger than the diameter of a typical SWNT (≈1–2 nm), the maximum number of columns that the individual nanotube electrode can contact is 2, even considering significant fringing fields near the electrodes. Given the size of the gap and the volume of the molecules assembled in this gap, we can estimate that the collective properties of ≈4–12 molecules are being probed (assuming that the molecule pack is ≈0.5 nm, face-to-face, and is ≈2.5 nm in diameter) (22, 23).

It is remarkable to note again that the electrical properties of these devices after annealing have been significantly improved. These molecular transistors, which have the 1D ballistic SWNTs as point contacts, exhibit the high current modulation and high on/off ratio. The on/off ratio is as high as >3 orders, which is difficult to achieve in ultrasmall devices in comparison with

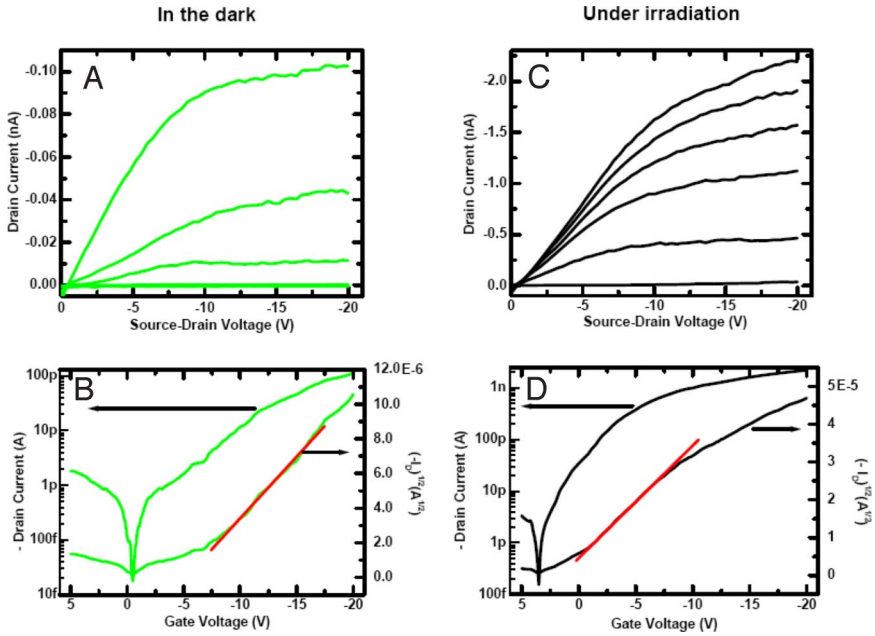

Fig. 4. Device characteristics of a device made by drop-casting in the dark and under irradiation with visible light after annealing. The electrical characteristics of the original tube before and after oxidative cutting can be viewed in Fig. S2. (*A*) Transistor output, V_G = 0 to −20 V in 4-V steps. (*B*) Transfer characteristics for the device, V_D = −20 V. (*C*) Transistor output, V_G = 0 to −20 V in 4-V steps for the same device under irradiation. (D) Transfer characteristics for the device, V_D = −20 V.

metallic S/D electrodes (26–28). This is because of the 1D nature of SWNT electrodes in the devices. In such devices, the electric field around SWNT/junction regions can concentrate at a point and then efficiently penetrate into the middle of the channel where single columns of HBCs locate and enable the observed high on/off ratio. Similar highly switching devices have been reported on other cases using 1D SWNT electrodes (9, 16). In addition to the 1D nature of SWNTs, we also think self-assembled columnar nanostructures of HBCs play an important role in device performance. Self-assembly allows HBCs to self-organize into columnar structures, which have a similar diameter to that of SWNTs, for forming the active channels. By comparing the electrical properties of the same devices before and after annealing, we infer that a single column used for bridging the nanogaps of SWNT electrodes will make the main contribution to device conductivity. In comparison with the cases using SWNT electrodes for detecting pentacene FET properties (9, 16), these devices made from SWNT electrodes and HBC columns are robust and can survive the measurement of much higher S/D voltage bias, such as −11 V in Fig. 3, or even higher, −20 V in Fig. S1. The subthreshold swing (S) in the device in Fig. 3*D* after annealing is ≈500 mV per decade, which is similar to the values obtained by Dai's group (9) and ours (22). Despite the similarity, our devices can turn on at an obvious lower gate electric field even though we still use a thick silicon oxide layer (300 nm). By using a similar method to that used before (22), the calculated carrier mobility is quite high, >1 $cm^2/V{\cdot}s$.

Photoresponsive Properties. A significant feature of HBCs is the presence of their 2 separate π systems: the conductive planar radialene core and the insulating alkoxyphenyl sheath (Fig. 1*A*). When the liquid crystalline columns are exposed to visible light, photoconductivity can be measured, originating from photoexcitations that are restricted in the hexaradialene core by the insulating alkoxyphenyl cladding (25). The path of photocurrent is dominated by intracolumnar transport through the 1D redialene core. In this study, we use SWNTs as point contacts to measure the photoconductivity of an individual 1D liquid crystalline columnar core because the size of these columnar nanostructures perfectly matches the diameter of SWNT electrodes. Fig. 4 shows the comparison of the electrical characteristics of the same annealed device made by drop-casting in the dark and under the irradiation of visible light. For the electrical characteristics of the original tube before and after oxidative cutting, see *SI Text*. We measure DC photoconductivity at room temperature in ambient atmosphere by illuminating the devices with visible light from a 150-W halogen lamp. In both cases, the devices show the typical *p*-type FET properties. We notice that the source-drain current (I_D) of the device under illumination increases to ≈20 times its original value in the dark (Fig. 4 *A* and *C*). Fig. 4 *B* and *D* shows the source-drain current (I_D) as a function of the gate voltage (V_G) while the source-drain bias voltage (V_D) is held at −20 V. In addition to the large current increase described above, the threshold voltage (V_T) of the device shifted from approximately −0.4 V in the dark to approximately +3.5 V under light illumination (Fig. 4 *B* and *D*), implying that light can significantly fine-tune the electrical conductivity of these molecular electronic devices. Both of the changes in current and V_T are universal for each working device. From the drop in current in the different conditions, the resistance and therefore the molecular column conductance can be estimated. In this case, the metallic tube bridged by HBC column in Fig. 4 goes from a resistance of $\approx 4.80 \times 10^5\ \Omega$ before cutting (Fig. S2) to $\approx 1.76 \times 10^{11}\ \Omega$ after connection in the dark and then to $\approx 8.99 \times 10^9\ \Omega$ upon exposure to light in the linear response regime. This yields a molecular conductance for HBC in this device of $1.47 \times 10^{-7}\ e^2/h$ in the dark and $3.03 \times 10^{-6}\ e^2/h$ upon exposure to light. We suppose that these significant photoresponses of the nanojunctions are ascribed to the photoexcited states of HBC columns, which greatly increase the transistor carrier density, improving charge transport mobility.

To monitor the photocurrent of the devices in real time, as shown in Fig. 5, we measured the drain current as a function of time of the same device used above while it was held at −20 V source-drain bias and −8 V gate bias by switching on/off light.

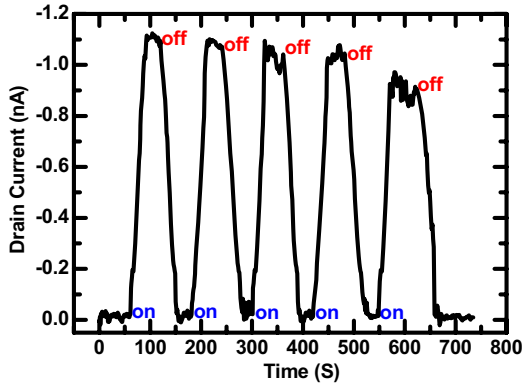

Fig. 5. The drain current as a function of time whereas the same device measured in Fig. 4 is held at −20 V source-drain bias and −8 V gate bias by switching on/off light.

We noticed that the response time is slow, ≈30 seconds, probably because of the diffusion processes and/or large capacitive components. The reversible photocurrent degraded a little after several cycles because of the presence of oxygen and moisture in the air. However, the switching ratio is as high as >3 orders, similar to that reported previously in the case of metal nanojunctions (29). The calculated responsivity of the device is also very high, $\approx 8.10 \times 10^5$ A/W at an intensity of 30 mW/cm^2 (assuming $W = 1.5$ nm and $L = 3$ nm, $V_D = -20$ V and $V_G = -8$ V). However, this value is just for comparison with conventional photodetectors (typically <10 A/W) (30, 31) because we use the same conventional model for the calculation (32), which is not accurate here. The power dependence of the photocurrent of another working device can be seen in Fig. S3. With the increase of light power, the drain current of the device gradually saturates, indicating that the photoinduced carrier density reaches its maximum.

To ensure that the path of photocurrent is through the nanojunctions between SWNT electrodes and HBC columns (15, 17) we also tested devices that have been fully cut but lack HBC molecules. All of these devices behave as open circuits with no field effect induced by the gate electrode. To further understand the important role of HBCs in device photoconductivity, we intend to display the wavelength-dependence measurement of the devices. The current responses as a function of light wavelength of a device made by drop-casting have been shown in Fig. S4 while the device is held at −20-V source-drain bias and 0-V gate bias. The peaks of the photocurrent spectral response of the device at ≈400 nm match those of the UV/vis absorption spectrum of HBC thin films because of the "radialene" π–π^* transitions (25). Because of the combinations of vibronic excitations, there are several overlapping peaks. The weak peaks at >450 nm in the red curve are most likely due to (radialene π) − (radialene π^*) triplets. These results, as well as V_T shifts and conductance changes discussed above, without doubt prove that self-assembled columnar nanostructures of HBC molecules play the key role in device characteristics.

Finally, to identify the universality of the device photoresponsibility, we choose another organic semiconductor 6,13-di(2′-thienyl)pentacene to do the similar experiments. In this case, we use the device geometry in Fig. 1*B* and then deposit the materials on the top of the substrate through thermal evaporation. An advantage of this molecule is its cofacially arranged π–π stacking crystal structure (33), which will make a nice contact between SWNT electrodes and molecules (Fig. S5*A*). This is important to improve the device properties (9, 16, 22). Fig. S6*A* shows an optical photograph of a device used with SWNT–metal junctions protected by HSQ. All of the working devices exhibit the typical *p*-type FET properties. A set of experimental data is available in Fig. S5. In the photocurrent experiments, we also observed the large current increases of the devices upon exposure to visible light because of the photoexcited states of the molecules. As shown in Fig. S7, the drain current of the device gradually increased with the increase of light power. The other data of this device can be found in Figs. S6 and S7. The important finding here is that these devices are ultrasensitive to light and chart a clear and universal path of making efficacious light-to-current converter in the future.

Summary and Perspectives

This work demonstrates a universal methodology of how to integrate molecular functionalities into molecular electronic devices through combination of top-down device fabrication and bottom-up self-assembly. By using 1D ballistic single-walled carbon nanotubes as point contacts, we are able to make stable high-performance molecular FETs from self-assembled liquid crystalline columns of contorted aromatic HBCs. Because of the presence of the active HBC molecules, these devices are very sensitive to their environmental stimuli, such as temperature and photons. These efficacious stimuli-responsive nanoscale columnar transistors should have the broad potential applications in ultrasensitive devices for environmental sensing and solar energy harvesting. In addition integration with SWNT electrodes to develop ultraminiature optoelectronic devices with molecular sizes in all dimensions could lead to important application in nanoscience and molecular electronics.

Materials and Methods

SWNT Transistor Fabrication. Individual SWNTs of high electrical quality were grown by a chemical vapor deposition (CVD) process from a CoMo-doped mesoporous SiO_2 catalyst particles process using ethanol as the carbon source (34–35). The catalyst particles were patterned onto doped silicon wafers that have 300 nm of thermally grown SiO_2 on the surface. Source and drain electrodes (5 nm of Cr followed by 50 nm of Au) separated by ≈20 μm were deposited through a metal shadow mask onto the carbon nanotube samples by using a thermal evaporator. The doped silicon wafer serves as a global back-gate electrode for the samples. After the initial electric characterization, we selected individual metallic carbon nanotube devices to do all of the following experiments.

Cutting Procedure. SWNT electrodes are made through the procedure described previously (18–22). The details of the procedure can be also found in *SI Text*. Under these optimized conditions, ≈20–25% of the tubes were completely cut. Based on the previous results (18–22), the statistical variability of the plasma etch process creates ensembles of nanotube devices with gaps in the 1- to 10-nm range. Parts of the devices were used further to fabricate the devices with SWNT–metal junctions protected by HSQ by using e-beam lithography according to our previous report (17).

Columnar Transistor Formation. Tetradodecylhexabenzocoronene (HBC) (Fig. 1) was synthesized according to our previous procedure (23). After the nanogaps between carbon nanotubes were ready, films were deposited by spin-casting, or a tiny drop was formed by using a picospritzer immediately from 1,2-dichloroethane (concentration 1 mg/ml, 1200 rpm, 20 seconds; IMECAS Model KW-4A). It should be noted (23) that a heating/cooling cycle can promote self-assembly or self-healing of contorted HBCs to form an ordered columnar liquid structure bridging the nanogaps between carbon nanotubes. Unless otherwise noted, all of the nanodevices used in this article were pretreated by heating to 125 °C and cooling down to room temperature before full electrical characterization.

Transistor Characterization. The transistor characterization of nanoscale columnar transistors was carried out at room temperature in the ambient atmosphere by using an Agilent 4155C semiconductor characterization system and a Karl Suss (PM5) manual probe station. To initiate the maximum photocurrent, we used the white light of the probe station to characterize their optoelectronic properties. As for the source-drain current (I_D) vs. wavelength experiments, the device was illuminated with visible light (370–700 nm) coming from a xenon lamp. Details are published in *SI Text*.

ACKNOWLEDGMENTS. We thank Philip Kim, Yunqi Liu, Shalom J. Wind, Yaron Cohen, and Etienne De Poortere for enlightening discussions and Limin Huang and Stephen O'Brien for assistance in the growth of SWNTs. We acknowledge primary financial support from the Nanoscale Science and Engineering Initiative of the National Science Foundation (NSF) under NSF Award CHE-0117752 and by the New York State Office of Science, Technology, and Academic Research (NYSTAR) and NSF Award ECCS-0707748. X.G. thanks the New Faculty Start-up Funds from Peking University, FANEDD (No. 2007B21) and National Natural Science Foundation of China Grants 50873004 and 20833001 for financial support. C.N. thanks NSF CAREER award (DMR-02-37860). We thank the Materials Research Science and Engineering Center Program of the National Science Foundation under Award DMR-0213574 and NYSTAR for financial support for M.L.S. and the shared instrument facility.

1. Tour JM (2000) Molecular electronics. Synthesis and testing of components. *Acc Chem Res* 33:791–804.
2. Flood AH, Stoddart JF, Steuerman DW, Heath JR (2004) Chemistry. Whence molecular electronics? *Science* 306:2055–2056.
3. Heath JR, Ratner MA (2003) Molecular electronics. *Phys Today* 56:43–49.
4. Ramachandran GK, *et al.* (2003) A bond-fluctuation mechanism for stochastic switching in wired molecules. *Science* 300:1413–1416.
5. Metzger RM (2003) Unimolecular rectifiers and proposed unimolecular amplifier. *Ann NY Acad Sci* 1006:252–276.
6. Nitzan A, Ratner MA (2003) Electron transport in molecular wire junctions. *Science* 300:1384–1389.
7. Ajayan PM, Iijima S (1992) Smallest carbon nanotube. *Nature* 358:23–25.
8. Someya T, Kim P, Nuckolls C (2003) Conductance measurement of single-walled carbon nanotubes in aqueous environment. *Appl Phys Lett* 82:2338–2340.
9. Qi P, *et al.* (2004) Miniature organic transistors with carbon nanotubes as quasi-one-dimensional electrodes. *J Am Chem Soc* 126:11774–11775.
10. Dai H (2002) Carbon nanotubes: Synthesis, integration, and properties. *Acc Chem Res* 35:1035–1044.
11. Someya T, Small J, Kim P, Nuckolls C, Yardley JT (2003) Alcohol vapor sensors based on single-walled carbon nanotube field effect transistors. *Nano Lett* 3:877–881.
12. Kong J, Soh HT, Cassell AM, Quate CF, Dai H (1998) Synthesis of individual single-walled carbon nanotubes on patterned silicon wafers. *Nature* 395:878–881.
13. Postma HW, Teepen T, Yao Z, Grifoni M, Dekker C (2001) Carbon nanotube single-electron transistors at room temperature. *Science* 293:76–79.
14. Collins PG, Arnold MS, Avouris P (2001) Engineering carbon nanotubes and nanotube circuits using. electrical breakdown. *Science* 292:706–709.
15. Star A, Lu Y, Bradley K, Gruener G (2004) Nanotube optoelectronic memory devices. *Nano Lett* 4:1587–1591.
16. Tsukagoshi K, Yagi I, Aoyagi Y (2004) Pentacene nanotransistor: Pentacene nanocrystal connected by carbon nanotube electrodes. *Appl Phys Lett* 85:1021–1023.
17. Guo X, Huang L, O'Brien S, Kim P, Nuckolls C (2005) Directing and sensing changes in molecular conformation on individual carbon nanotube field effect transistors. *J Am Chem Soc* 127:15045–15047.
18. Guo X, *et al.* (2006) Covalently bridging gaps in single-walled carbon nanotubes with conducting molecules. *Science* 311:356–359.
19. Guo X, *et al.* (2007) Single-molecule devices as scaffolding for multicomponent nanostructure assembly. *Nano Lett* 7:1119–1122.
20. Whalley AC, Steigerwald ML, Guo X, Nuckolls C (2007) Reversible switching in molecular electronic devices. *J Am Chem Soc* 129:12590–12591.
21. Guo X, Gorodetsky AA, Hone J, Barton JK, Nuckolls C (2008) Conductivity of a single DNA duplex bridging a carbon nanotube gap. *Nat Nanotech* 3:163–167.
22. Guo X, *et al.* (2006) Chemoresponsive monolayer transistors. *Proc Natl Acad Sci USA* 103:11452–11456.
23. Xiao S, *et al.* (2005) Molecular wires from contorted aromatic compounds. *Angew Chem Int Ed* 44:7390–7394.
24. Xiao S, *et al.* (2006) Transferring self-assembled, nanoscale cables into electrical devices. *J Am Chem Soc* 128:10700–10701.
25. Cohen YS, Xiao S, Steigerwald ML, Nuckolls C, Kagan CR (2006) Enforced one-dimensional photoconductivity in core-cladding hexabenzocoronenes. *Nano Lett* 6:2838–2841.
26. Tulevski GS, *et al.* (2004) Attaching organic semiconductors to gate oxides: In situ assembly of monolayer field effect transistors. *J Am Chem Soc* 126:15048–15050.
27. Dimitrakopoulos CD, Malenfant PRL (2002). Organic thin film transistors for large area electronics. *Adv Mater* 14:99–117.
28. Kagan CR, Andry P (2003). *Thin-Film Transistors* (Dekker, New York).
29. Hu W, *et al.* (2005) A self-assembled nano optical switcher and transistor based on a rigid conjugated polymer thioacetyl-end-functionalized poly(para-phenylene ethynylene. *J Am Chem Soc* 127:2804–2805.
30. Lai K-S, Huang J-C, Hsu KY-J (2007) High-responsivity photodetector in standard SiGe BiCMOS Technology. *IEEE Elec Device Lett* 28:800–802.
31. Garrett LD, Qi J, Schow CL, Campbell JC (1996) A Silicon-based integrated NMOS-p-i-n photodetector. *IEEE Trans Elec Devices* 43:411–416.
32. Hamilton MC, Martin S, Kanicki J (2004) Thin-film organic polymer phototransistors. *IEEE Trans Elec Devices* 51:877–885.
33. Miao Q, *et al.* (2006) Organization of acenes with a cruciform assembly motif. *J Am Chem Soc* 128:1340–1345.
34. Huang L, Cui X, White B, O'Brien SP (2004). Long and oriented single-walled carbon nanotubes grown by ethanol chemical vapor deposition. *J Phys Chem B* 108:16451–16456.
35. Huang L, Wind SJ, O'Brien SP (2003). Controlled growth of single-walled carbon nanotubes from a line patterned mesoporous silica template. *Nano Lett* 3:299–303.